The formation of an expanding memory representation in the hippocampus

Sachin P. Vaidya, Raymond A. Chitwood & Jeffrey C. Magee

Howard Hughes Medical Institute, Baylor College of Medicine, Houston, TX, 77030

Correspondence to: Jeffrey C. Magee

HHMI/Baylor College of Medicine

Jan and Dan Duncan Neurological Research Institute

1250 Moursund Dr., Houston, TX, 77030, USA

Email: jcmagee@bcm.edu

Abstract

How episodic memories are stored within brains is poorly understood. While certain memory-retaining neurons have been potentially identified[1-3], it is unclear if they retain learned information[4,5]. Further, there is considerable evidence that neuronal activity is unstable and may require additional mechanisms to support robust memory[6-11]. To examine these issues, we recorded the activity of a hippocampal CA1 neuronal population for 7 days as mice learned cued reward locations. These data and modelling results suggest that two place cell (PC) pools, distinguished by place field (PF) stability, are formed each day (transient: ~1.5 days; sustained: ~2 weeks)[8]. Notably, the proportions of these pools changed across the week as unstable transient PCs were progressively replaced by sustained PCs, markedly enhancing the stability of the total representation. This growing stable representation contained behaviorally relevant information and sustained PCs became active immediately at the start of each session. Finally, the initial formation of sustained PCs was associated with a higher rate and efficacy of behavioral timescale synaptic plasticity (BTSP) and these PCs showed elevated and more reliable activity. It, therefore, appears that BTSP stabilizes particularly informative PCs, incorporating them into an expanding and readily retrievable representation that displays hallmarks of a long-lasting memory.

Any beneficial information learned by animals during a behavioral episode should be retained and later retrieved during similar experiences[12,13]. Within the hippocampus, learning during an experience produces environment-specific population activities (context discriminability)[14-16] that include high densities of PCs at reward sites and salient feature locations (over-representations) [17-21]. The retrieval of a stored memory of this experience should be observable as correspondingly structured population activity on subsequent days of similar experience.

There is evidence, primarily from neuronal tagging studies (e.g., immediate early genes; usually c-Fos), that such a memory retrieval, and by implication, storage process may occur in a population of active hippocampal place cells (PCs)[1-3]. Yet it is not clear from these and other studies if the tagged neurons contain the experience-dependent information learned by the hippocampus (i.e., the discriminability and over-representations)[4,5]. In addition, many longitudinal studies that followed populations of PCs for days report that the hippocampal

population code is relatively unstable, with only a small fraction of the same PCs remaining active over a week-long exposure to the same behavioral environment[6-11]. Therefore, how episodic memories are stored in sparse neuronal populations within the hippocampus remains poorly understood.

We used two-photon Ca^{2+} imaging to longitudinally record the activity of a single hippocampal CA1 neuronal population for 7 days as head-fixed transgenic mice expressing GCaMP6f[22] learned two separate reward locations on a linear treadmill that was enriched in tactile features (2511 total pyramidal neurons tracked; 126±5 laps/session; 70 sessions over 7 days in 10 mice) (Fig. 1a; Extended Data Fig. 1). The mice were first habituated on a featureless track as a sucrose-water reward was delivered at random locations. On day 1, the habituated mice were exposed to a new feature-containing track with two alternating reward locations given in 12-18 lap blocks. Reward location was contingent on a specific light cue given to either the left or right eye at a set location (Fig. 1b). Behavioral performance, as assessed by running and licking patterns improved over the 7 days (Fig. 1c-e). Both single neuron (Fig. 1f&g; Extended Data Fig. 2a) and population (Fig. 1h; Extended Data Fig. 2b) PC activity also evolved over the recording days such that by day 7 two highly distinct and stable neuronal activity patterns had developed (discriminability), each with its own PC spatial density profile (over-representations) (Fig. 1i; Extended Data Fig. 2).

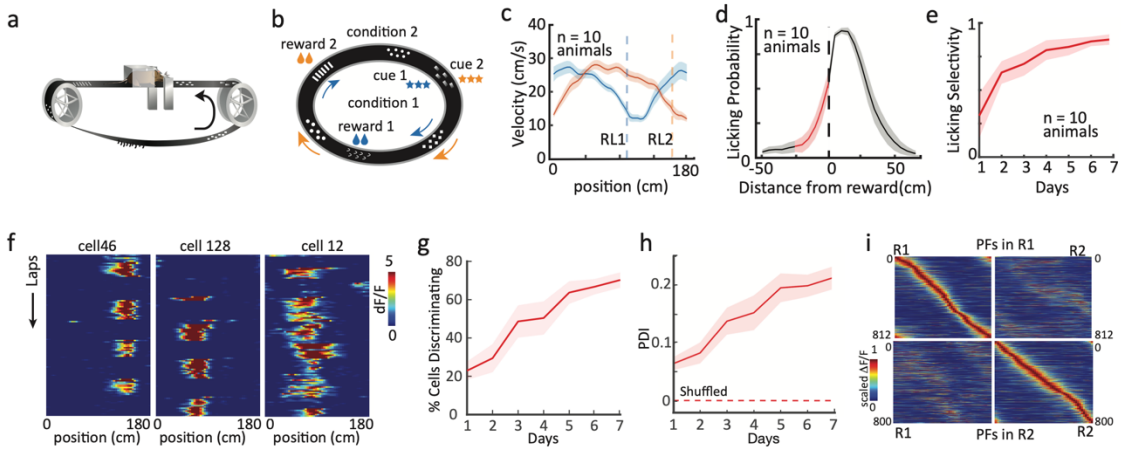

Fig. 1: Daily evolution of behavior, single neuron and population activity. a, Schematic of experimental apparatus and (**b**) two different cue-reward location conditions. **c,** Average velocity profiles for mice during condition RL1 (blue; shading is SEM) and RL2 (orange) on day7. Note selective slowing near reward locations. **d,** Licking probability in reference to reward locations with anticipatory licking shown in red for day 7. **e,** Licking selectivity (see Methods) as a function of behavior day. **f,** example PCs with RL2 preference, RL1 preference, and no preference (left to right). **g,** Percentage of PCs showing high cell discriminability increased across experimental days. **h,** Population discriminability index (PDI) increases with experimental day. Dashed line shows PDI for shuffled data. **i,** Heat maps of PCs with PF activity in condition RL1 (top), during RL1 (top left) and RL2 (top right; both sorted by

activity during RL1). Bottom, same as top but for PC with PFs active in condition RL2 (sorted by activity during RL2).

To look for the formation of a memory representation in this neuronal population we tracked active PCs on each experimental day for the entire week (see methods for PC criteria). The total population of active PCs for any given day was relatively constant (average PC count/day from 10 mice combined=767±8 PCs, n=14; for 2 reward location (RL) conditions over 7 days; PCs are 30.5% of imaged pyramidal neurons). For PCs active on Day 1 we observed that those maintaining a consistent PF location for all of the consecutive days decreased progressively from ~35% on the next day (day 2) to ~6% by day 7 (Fig. 2a) (PF center of mass (COM) on each subsequent day within ±30 cm of location on the first day; see methods and Extended Data Fig. 3). Performing this same analysis for each of the subsequent days (i.e., days 2-7) showed a similar rate of decrease in PC counts for each day (Fig. 2a). The decay of consistently active PCs that first appeared on days 1&2 were well fit by double exponential functions (t_{fast}=0.67±0.02 day; t_{slow} =4.6±0.19 days; n=4, 2 RL conditions for each day; Fig. 2a; Extended Data Fig. 3). This suggests the presence of two separate pools of PCs that can be distinguished by the duration over which they maintain a consistent PF on consecutive days[20]. Further, the enhanced stability of a set of PCs (presumably those producing τ_{slow}) resulted in an accumulation of PCs that had first appeared on previous days (past PCs), while the number of newly appearing PCs (new PCs) decreased through the week (Fig. 2b-e). The quantity of past PCs was much higher than expected from a random memoryless process suggesting that these PCs are part of an expanding memory representation (data; pastPC total=2284 vs expected=490; Fig. 2d; Extended Data Fig. 2).

All aspects of the above process were adequately captured by the dynamics of a competitive interaction between three pools of model "neurons", which simulated (1) available pyramidal cells, (2) transient cells and (3) sustained cells (see Methods; Extended Data Fig. 4a-e). The different decay rates in the model (based off the double exponential fits in Fig. 2a) produced a sustained group that decayed back to the available population nearly an order of magnitude more slowly (τ_{sust}=4.6 days) than the transient population (τ_{trans} = 0.67 days) (Extended Data Fig. 4f&g). The resulting accumulation of the sustained model cell group over 7 days simulated the activity of real PCs (Fig. 2f) and the model results accurately predicted the PC counts over the week (MSE= 182, n=28; Fig. 2g).

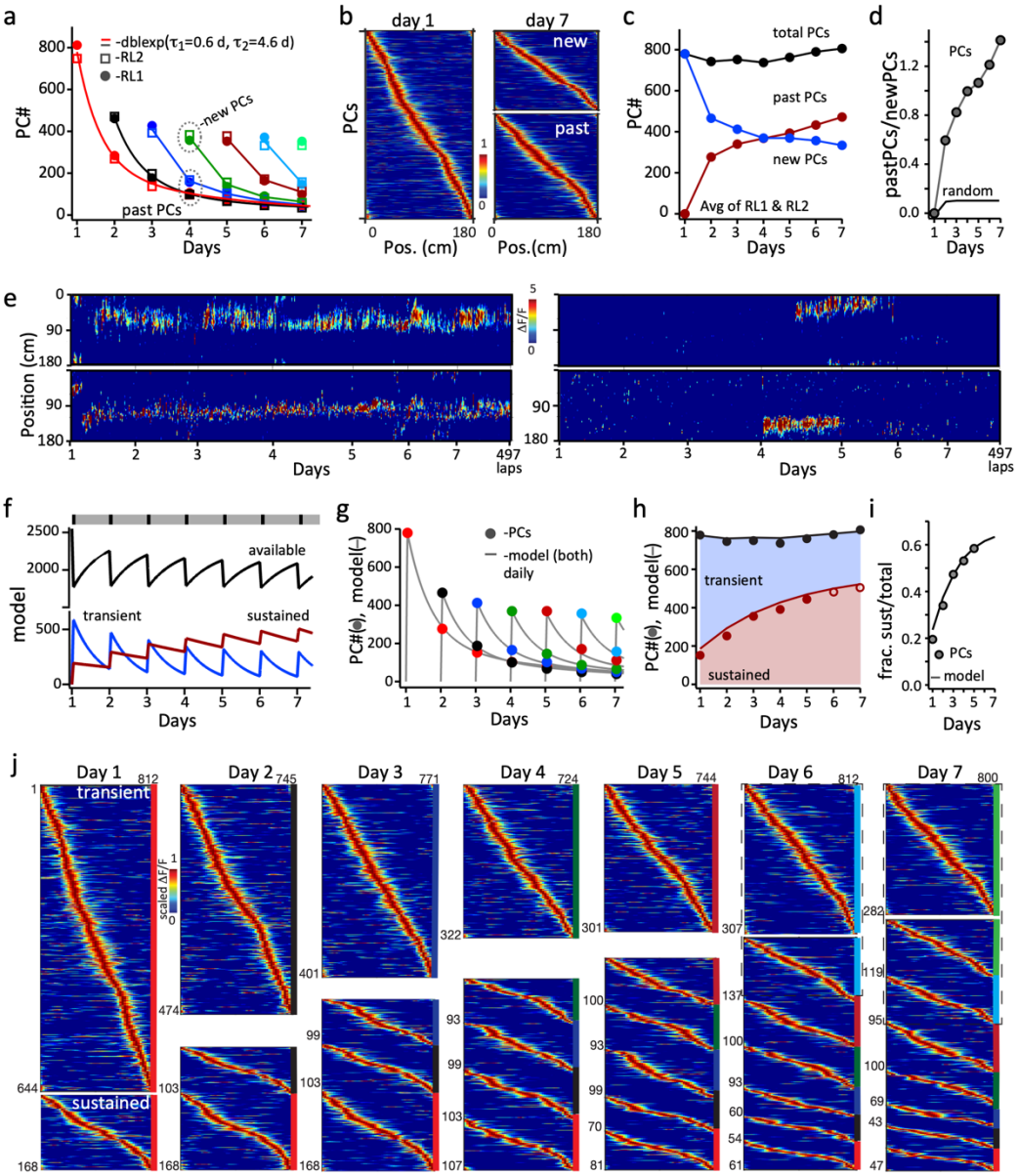

Fig. 2: Two pools of PCs are formed each day. **a,** counts for PCs that first appear on day 1 and maintained a consistent PF on subsequent days (consistent PF present on each day from 1 through 7; red). Other colors are PCs that first appear on days 2-7 and maintained a consistent PF on subsequent days (day 2, black; day 3, dark blue; day 4, dark green; day 5, dark red; day 6 light blue; day 7, light green). PCs during RL1 (squares) and RL2 (circles). Solid lines over PC counts for days 1 and 2 are double exponential functions produced by fits of data. **b,** (left) PCs active on day 1 sorted by PF location, (right) PCs active on day 7 separated into new PCs (upper; have not maintained consistent PF) and past PCs (lower; maintained consistent PF from previous days), sorted by PF location on day 7. **c,** PCs divided into past PCs (red) and new PCs (blue) plotted against experimental day. All PCs (which is equal to the sum of past and new PCs; black) versus experimental day. PC counts are the average of RL conditions. **d,** Ratio of past PC to new PC counts for each experimental day (Gray circles). Calculated ratio from random process (black line; Extended Data Fig. 3). **e,** Example PCs. **f,** Model cell counts for transient (blue), sustained (red) and available (black) pools for continuous model run for 7 days. At top, 1 hour on-track, (100 time-steps for activation; Black rectangles) and 23 hours off-track (2300 timesteps for decay; gray rectangles) are shown for each day. **g,** PC numbers (average of two RL conditions), color scheme same as panel b. Gray lines are from single day runs of model with sustained and transient components combined (both; see Extended Data Fig. 4g). MSE =182. **h,** PC counts for sustained group

(red circles) and sustained population model estimate (red line), total PC count (black circles) and total model pool count (black line), blue shading is transient model pool count and red shading is sustained model pool count. Open circles on days 6&7 indicate predictions from model. **i,** Fraction of total PCs count that are sustained PCs versus experimental days (circles) and model predictions (line). **j,** Visualization of transient PCs and sustained PCs evolution for each experimental day using PC activity heat maps for each group sorted by PF location in that population. Color bars on sides are coded according to (**a**). PCs from RL2 condition and total counts are shown at top. Dashed line on days 6 and 7 indicates where cell counts were inferred from model.

The presence of two very different PC stabilities suggests a relatively straightforward method for isolating PCs into separate populations based on the number of days that they maintained consistent PFs (transient PCs ≤ 2 days; sustained PCs > 2 days; Extended Data Fig. 4f). Using this method to separate the model pools, which have a known identity, predicts only a small error in the numbers of PCs assigned to each group (mean error =6.9%; Extended Data Fig. 4h). We thus separated the actual PCs present on each experimental day and the accumulation of PCs within the sustained group at the expense of the transient population was readily observable (Fig. 2h-j). Indeed, the proportion of the total active PC population provided by sustained PCs increased nearly three-fold after 5 days of repeated learning and this was significantly correlated with a similar increase in the stability of the total PC population over the same days (Fig. 2i; Extended Data Fig. 5a-c). Together, these data suggest that two populations of PCs are active on each day, one that rapidly becomes inactive or with altered PF tuning, and another much more stable population that appears to be added to a progressively expanding memory representation of the animal's past experience.

For the sustained PCs to function as a memory of what was previously learned we would expect to find properties of the sustained representations that reflect the animals prior experience. Thus, we determined the spatial density profiles of the two groups of PCs (Fig. 3a) and found that the PC density (PC count/cm) around salient regions (reward and cue) was substantially more elevated in the sustained group than in the transient population (see confidence intervals in Fig. 3b, Extended Data Fig. 5d,e)[20]. In addition, we determined the level at which each individual neuron (CDI) as well as the entire population (PDI) was able to discriminate the two different reward conditions and found that sustained PCs were more discriminative than transient (mean CDI; sustained:0.172±0.003, n=2455 cells, transient:0.089±0.002 n=1874 cells, $p=<1.0e^{-7}$ unpaired two-tailed students t-test; mean PDI; sustained: 0.14±0.02, n=10 mice, transient: 0.09±0.01 n=10 mice, $p=1.0e^{-3}$ paired two-tailed students t-test; Fig. 3c-e, Extended Data Fig. 5f). Thus, the experience-dependent development of both the spatial over-representation of salient

regions and reward condition discrimination were found to be markedly elevated in the sustained over the transient PC group.

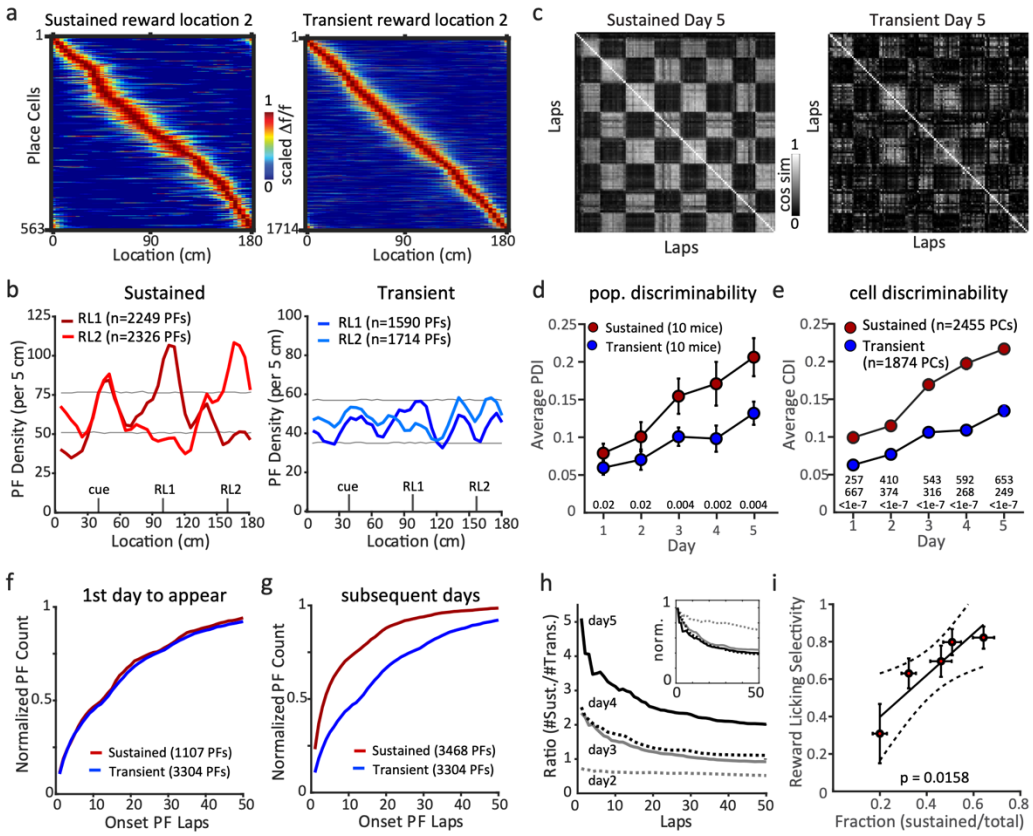

Fig. 3: Properties of sustained and transient PC groups. a, PC activity heatmaps for sustained (left) and transient (right) groups under RL2 condition days 1-5 combined. **b,** PF densities for sustained PCs (left, red) and transient PCs (right, blue) under RL1(dark colors) and RL2 (light colors) conditions. Gray lines are 99% confidence intervals of random distribution produced via bootstrapping 10,000 times. Sustained groups include identified PFs from days 1-7 and transient groups includes identified PFs from days 1-5. **c,** Cosine similarity matrices for sustained (left) and transient (right) populations on day 5 from a single mouse. **d,** Population discriminability (PDI) versus experimental day, p- values from two-way, paired t-tests are shown for each day. **e,** cell discriminability (CDI) versus experimental day, n- (sustained, upper; transient, middle) and p- values (lower) from two-way, unpaired t-tests are shown for each day. **f,** Cumulative distribution of onset lap (first trial PC appeared) for the first days that PC appeared for sustained (days 1-5) and transient groups (days 1-6). **g,** Sustained group on subsequent days (2-7). Transient group is same as in panel (**f**). **h,** Ratio of number of sustained PCs to number of transient PCs for a given lap for days 2-5 (gray dashed day 2; gray solid, day 3; black dashed, day 4; black solid, day 5). Inset shows ratios normalized to the peak amplitude of each day. **i,** Reward licking selectivity versus fraction of total population that is composed of sustained PCs. P-value for linear regression is shown.

We next asked if the sustained population was active over the same range of trials during a given behavioral session as the transient population. We found that while the range of PC onset trial was similar between the two groups on the first day that a PC appeared (KS test p = 0.9541; Fig. 3f, Extended Data Fig. 5g), on all subsequent days the sustained PCs became active much earlier in the session than the transient population (KS test p = 3.63e-06; Fig. 3g; Extended Data

Fig. 5h). This caused the fraction of the total representation contributed by the sustained population to be higher at the beginning of each session, particularly on later days (Fig. 3h). Thus, stable PCs appear to be immediately retrieved into activity during each new day's experience. Finally, we found that the daily increase in the selectivity of licking that occurred across the week of behavior was highly correlated with the proportion of the total PC population made up of sustained PCs on a given day (Fig. 3i Extended Data Fig. 5i). These data suggest that the daily rapid retrieval of a growing memory representation could contribute to the progressive enhancement of the behavior observed in these mice.

To investigate what mechanisms might be responsible for the different levels of stability observed in the above two populations we more closely examined the activity of each PC on the first day that it became active (first day of appearance). Specifically, we looked for the known signatures of behavioral timescale synaptic plasticity (BTSP) within each population[23-25]. BTSP is a directed form of synaptic weight plasticity that is induced when input from the entorhinal cortex (EC3) drives Ca^{2+} plateau potentials in the dendrites of CA1 neurons. Accumulating evidence suggests BTSP is the primary mechanism of PF formation and learning-related changes in CA1 population activity[23-28]. Here, we found that both the transient and sustained groups showed prominent signatures of BTSP induction on the first day of appearance (Fig. 4a-d; Extended Data Fig. 6a-i), suggesting that BTSP is involved in producing both PC pools. However, we also observed that the sustained population had a significantly higher average number of BTSP induction events per cell than the transient population (5-day mean, sustained; 1.02±0.02 events/cell, n=1107; transient 0.65±0.01 events/cell, n=2904; $p=<1.0e^{-7}$, unpaired two-tailed students t-test; Fig. 4e, Extended Data Fig. 6j). Consistent with a higher level of BTSP induction in the sustained PCs, we found that the sustained PCs had a larger PF amplitude in general, were more reliable from trial to trial and a given BTSP event induced a greater amount of PF potentiation (5-day mean amplitude; sustained; 1.25±0.02 ΔF/F, n=1107; transient 1.01±0.01 ΔF/F, n=2904; $p=<1.0e^{-7}$, unpaired two-tailed students t-test; Fig. 4f, Extended Data Fig. 6k; 5-day mean reliability, sustained; 0.72±0.006 fraction of active laps, n=1107; transient 0.58±0.004 fraction of active laps, n=2904; $p=<1.0e^{-7}$, unpaired two-tailed students t-test; Fig. 4g, Extended Data Fig. 6l; Event associated amplitude increase: sustained, 1.22±0.03 ΔF/F, n = 748; transient, 1.09±0.02 ΔF/F, n = 1475, p=0.0019, unpaired two-tailed students t-test; Extended Data Fig. 6a,d&i). Properties of BTSP induction events, which presumably reflect the somatic component

of the plateau potential, were either not significantly different or had minor differences (Sustained vs Transient: BTSP Event Duration (s): 3.88±0.37 vs 3.44±0.17: p=0.23; BTSP Event Amplitude (ΔF/F): 3.19±0.07 vs 2.95±0.05; p=0.008, unpaired two-tailed students t-test; Sustained n = 748, Transient n = 1475). These data indicate that, both in terms of frequency and efficacy, a greater amount of BTSP induction within a subset of PCs may produce the stable memory representation.

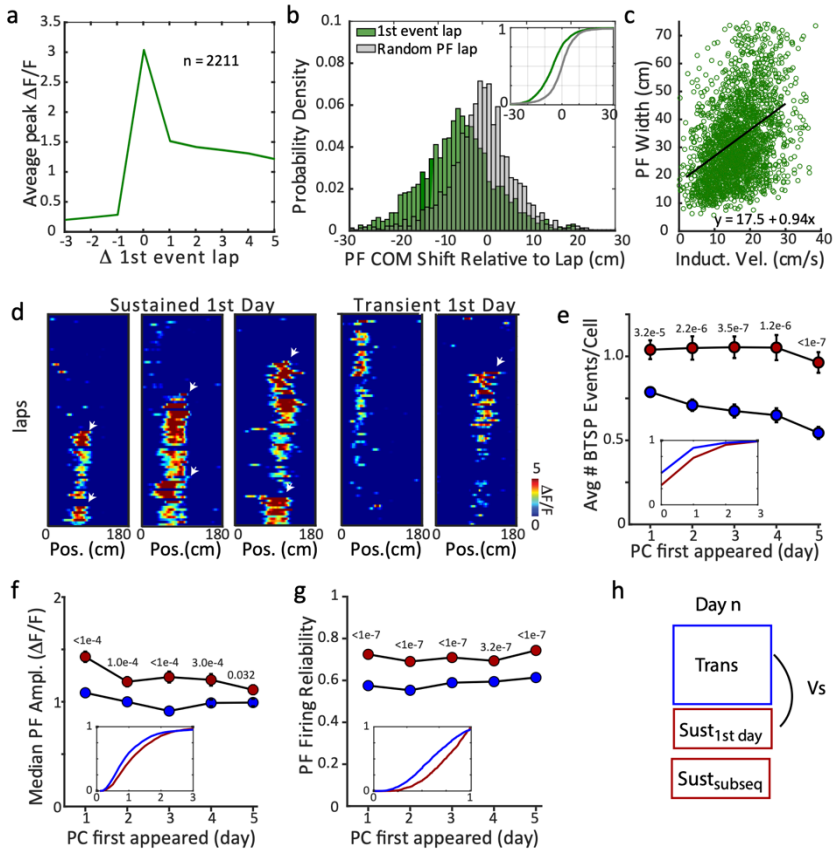

Fig. 4: Role of BTSP in producing sustained and transient PC pools. **a,** PC activity (sustained and transient combined) around BTSP induction event on the first day of appearance. Average activity aligned to trial where a large (20th percentile) Ca^{2+} signal associated with an increase in PF amplitude and reliability occurred. **b,** Histogram of PF center of mass shift for combined pools determined from part (**a**). **c,** Relationship between PF width and running velocity of mouse on event lap for PCs determined from part (**a**). **d,** Example of Sustained and Transient cells on first day of appearance. Only laps from one RL condition are shown. **e,** Average number of BTSP induction events per cell for sustained (red) and transient (blue) pools versus the first day of appearance (inset shows cumulative distributions for all days combined). **f,** Average PF amplitude for sustained (red) and transient (blue) PC pools versus the first day of appearance (inset shows cumulative distributions for all days combined) **g,** Average PF reliability for sustained (red) and transient (blue) PC pools versus the first day of appearance (inset shows cumulative distributions for all days combined). **h,** Schematic explaining that all comparisons are between transient and sustained groups for the first day of PC appearance. Ns for each day in (**e-g**): sustained 168, 271, 370, 392, 443; transient 644, 474, 401, 322, 301.

The results presented above suggest that BTSP-mediated learning produces two separate populations of PCs in hippocampal area CA1. One population, whose stable PF activity last approximately 36 hours, appears to collectively map spatial locations in the environment with a relatively low context discriminability. A second population, with a stability lasting for weeks, is composed of PCs whose activity showed a bias to salient regions of the environment and a high discriminability. Daily repeated learning causes the stable PC population to grow such that it is predominant by the end of one week's learning. Notably, this growing stable population maintains the information about the environment learned in the prior days and retrieval of this population is immediate at the start of a new day's behavioral session. This suggests a process that seeds the current day's representation with learned information from the animal's past experience. Finally, we found a strong correlation between the relative size of the stable memory representation and behavioral performance. Overall, we interpret these data to indicate that the sustained PC population is acting as an accumulating representation of past experience and that this long-lasting memory is beneficial for behavior.

The widely varying stability of the above PC pools is reminiscent of past theoretical work on the so-called synaptic plasticity-stability tradeoff present in network models of memory storage[29-31]. The obvious interpretation here would be that these two PC pools are produced by the induction of different levels of BTSP that, in turn, generates widely varying weight stabilities within a single type of synapses (e.g. the Schaffer collateral synapses from CA3 to CA1). However, future experiments should examine if there are actually two different types of synapses involved in producing the two pools of PCs. That is, perhaps the rapid and transient learning occurs by weight changes to one group (SC synapses) while a slower weight change, that is more resistant to overwriting, occurs within another (e.g. the perforant path synapses from EC3 to CA1). The similarity between the spatial density distributions of the sustained PCs and that of EC3 input to CA1 during similar experience reinforces this possibility[23]. Other questions relate to processes that could regulate the size and stability of the sustained population (i.e. alter the fraction of sustained PCs or τ_{slow}) such as different behavioral regimes, modulation of neuronal excitability, sleep and perhaps various neuropathologies[32-34]. In the end, our observations suggest that PCs with relatively stable synaptic weights produce an informative, readily retrievable, and progressively expanding memory representation in the mouse hippocampus. We also present

experimental methods for tracking this process and exploring its mechanisms that might be useful in further determining how episodic memories are formed in brains.

References and Notes

1 Liu *et al*. Optogenetic stimulation of a hippocampal engram activated fear memory recall. Nature 484, 381-385 (2012).

2 S. Ramirez *et al*. Creating a false memory in the hippocampus. Science 341, 387-391 (2013).

3 Tanaka, K.Z., Pevzner A., Hamidi A., Nakazawa, Y., Graham, J., Wiltgen, B.J. Cortical representations are reinstated by the hippocampus during memory retrieval. Neuron;84(2):347-54. (2014).

4 Tanaka, K.Z., *et al*. The hippocampal engram maps experience but not place. Science 361, 392-397 (2018).

5 Pettit, N.L., Yap, E-L, Greenberg, M.E. & Harvey C.D. Fos ensembles encode and shape stable spatial maps in the hippocampus. Nature 609, 327-334 (2022).

6 Ziv, Y., Burns, L., Cocker, E. *et al*. Long-term dynamics of CA1 hippocampal place codes. *Nat Neurosci* **16**, 264–266 https://doi.org/10.1038/nn.3329) (2013).

7 Hainmueller, T. & Bartos, M. Parallel emergence of stable and dynamic memory engrams in the hippocampus. Nature 558, 292-296 (2018).

8 Lee, J.S. *et al*. The statistical structure of the hippocampl code for space as a function of time, context and value. Cell 183, 620-635 (2020).

9 Grosmark A.D., Sparks, F.T., Davis, M.J. & Losonczy, A. Reactivation predicts the consolidation of unbiased long-term cognitive maps. Nature Neurosc, 24:1574-1585 (2021).

10 Keinath, A.T, Mosser, C.A. & Brandon M.P. The representation of context in mouse hippocampus is preserved despite neural drift. Nature Comm. 13,2415 (2022).

11 Driscoll, L, Duncker, L. & Harvey C. Representational drift: Emerging theories for continual learning and experimental future directions. Curr. Opin. Neurobiol. 76:102609 (2022.)

12 Eichenbaum, H. Still searching for the engram. Learn Behav 44:209-222 (2016).

13 Josselyn, S.A. & Tonegawa S. Memory engrams: Recalling the past and imagining the future. Science 367:1-14 (2020).

14 Markus EJ, Qin YL, Leonard B, Skaggs WE, McNaughton BL & Barnes CA. Interactions between location and task affect the spatial and directional firing of hippocampal neurons. *J Neurosci* 15:7079–7094 (1995).

15 Smith DM & Mizumori SJ. Learning-related development of context-specific neuronal responses to places and events: the hippocampal role in context processing. J Neurosci. Mar 22;26(12):3154-63. doi: 10.1523.3234-05.2006. PMID: 16554466 (2006).

16 Zhao, X., Wang, Y., Spruston, N., & Magee, J.C. (2020). Membrane potential dynamics underlying context-dependent sensory responses in the hippocampus. Nature Neurosci. *23*, 881–891.

17 Zemla, R., Moore, J.J., Hopkins, M.D. & Basu, J. Task-selective place cells show behaviorally driven dynamics during learning and stability during memory recall. Cell Reports 41,8, 111700 (2022).
18 Dupret, D., O'Neill, J., Pleydell-Bouverie, B. & Csicsvari, J. The reorganization and reactivation of hippocampal maps predict spatial memory performance. *Nat Neurosci* **13**, 995-1002, doi:10.1038/nn.2599 (2010).
19 Hollup, S. A., Molden, S., Donnett, J. G., Moser, M. B. & Moser, E. I. Accumulation of hippocampal place fields at the goal location in an annular watermaze task. *J Neurosci* **21**, 1635-1644 (2001).
20 Turi, G. F. *et al.* Vasoactive Intestinal Polypeptide-Expressing Interneurons in the Hippocampus Support Goal-Oriented Spatial Learning. *Neuron* **101**, 1150-1165 e1158, doi:10.1016/j.neuron.2019.01.009 (2019).
21 Zaremba, J. D. *et al.* Impaired hippocampal place cell dynamics in a mouse model of the 22q11.2 deletion. *Nat Neurosci* **20**, 1612-1623, doi:10.1038/nn.4634 (2017).
22 Dana, H. *et al.* Thy1-GCaMP6 transgenic mice for neuronal population imaging in vivo. *PLoS One* **9**, e108697, doi:10.1371/journal.pone.0108697 (2014).
23 Priestley, J. B., Bowler, J. C., Rolotti, S. V., Fusi, S. & Losonczy, A. Signatures of rapid plasticity in hippocampal CA1 representations during novel experiences. *Neuron*, doi:10.1016/j.neuron.2022.03.026 (2022).
24 Grienberger, C, & Magee J.C. Enthornal cortex directs learning-related changes in CA1 representations. *Nature* , doi:10.1038/s41586-022-05378-6 (2022).
25 Fan L.Z. *et al*. All optical physiology resolves a synaptic basis for behavioral timescale plasticity. Cell 186, 1-17 (2023).
26 Bittner, K. C., Milstein, A. D., Grienberger, C., Romani, S. & Magee, J. C. Behavioral time scale synaptic plasticity underlies CA1 place fields. *Science* **357**, 1033-1036, doi:10.1126/science.aan3846 (2017).
27 Bittner, K. C. *et al.* Conjunctive input processing drives feature selectivity in hippocampal CA1 neurons. *Nat Neurosci* **18**, 1133-1142, doi:10.1038/nn.4062 (2015).
28 Milstein, A. D. *et al.* Bidirectional synaptic plasticity rapidly modifies hippocampal representations. *Elife* **10**, doi:10.7554/eLife.73046 (2021).
29 Grossberg, S. Processing of expected and unexpected events during conditioning and attention: A pschophysiological theory. Psychological Review 89, 529-572 (1982).
30 Fusi, S., Drew, P.J. & Abbott, L.A. Cascade models of synaptically stored memories. Neuron 45, 599-611 (2005).
31 Lahiri, S. & Ganguli, S. A memory frontier for complex synapses. In Avances in neural information processing systems. pp-1034-1042 (2015).
32 Cai D.J. *et al*. A shared neural ensemble links distinct contextual memories encoded close in time. Nature 534,115-118 (2016).
33 Ryan, T.J. & Frankland, P.K. Forgetting as a form of adaptive engram cell plasticity. Nature Reviews Neuroscience. 23, 173-186 (2022).
34 Leal, S.L. & Yassa, M.A. Neurocognitive aging and the hippocampus across species Trends Neurosci., 38, pp. 800-812 (2015).

Online Methods

Mice and Surgery

All experiments were performed according to methods approved by the Baylor College of Medicine Institutional Animal Care and Use committee (Protocol AN-7734) and in compliance with the Guide for Animal Care and Use of Laboratory Animals. The data was collected from 29 GP5.17 mice of either gender (Jackson Laboratory, stock no. 025393). All experiments were performed in adult (>10 weeks) mice. Mice were housed under an inverse 12-hour dark/12-hour light cycle (lights off at 9 am) with temperature (~21 degrees Celsius) and humidity (~30-60%) control. All surgical procedures were performed under deep isoflurane anesthesia as described before[22]. After locally applying topical anesthetics, the scalp was removed, and the skull was cleaned. A 3 mm-diameter craniotomy was centered at 2.0 mm posterior from Bregma and 2.0 mm lateral from the midline above the hippocampus. Cortical tissue within the craniotomy was slowly aspirated under repeated irrigation with warmed sterile saline 0.9%. Once the external capsule was exposed, the cannula (3 mm diameter, 1.7 mm height) with a window (CS-3R, Warner Instruments) on the bottom was inserted and cemented to the skull. Finally, a custom-made titanium head bar was attached to the skull parallel to the plane of the imaging window using dental acrylic (Ortho-Jet, Lang Dental). Mice were given a recovery period of one week before any further behavioral training.

Behavioral Apparatus

A linear treadmill apparatus with stationary head-fixation posts and a self-propelled belt of length 180 cm was used to train the animals to run and perform subsequent behavioral experiments. The treadmill was equipped with rotary encoders that digitized the animal's position and velocity using Arduino- based microcontrollers. The location data was interfaced with a behavioral control system using a BPod module (Sanworks LLC) that delivered rewards through a solenoid valve (quiet operation, Lee valves) or light cues through an LED system at appropriate locations of the belt. All behavioral variables (position, velocity, lap markers, licks, trial types) were digitized at 10KHz via a PCIe-6343, X series DAQ system (National Instruments) using WaveSurfer software (wavesurfer.janelia.org).

Behavioral Task and Training

After a 7-day recovery period, mice were placed on water restriction (1.5ml/day). The behavioral training started with habituation to the experimenter for water rewards for 30 mins per day for at

least 5 days. The mice were then introduced to the treadmill and trained to run for water rewards at random locations on a blank belt with no sensory features. The mice were accustomed to the light cue (blue LED positioned in front of both eyes, flashing at 10 Hz for 500 ms) as well as 2-photon imaging during later parts of the training regime. The mice were trained for 5-7 days and had to run 100 laps in one hour before they were deemed ready to be introduced to the experimental task.

On day 1 of the behavioral task, the mice were introduced to a new featured belt (6 varying sensory cue patterns of approximately 15 cm equidistantly placed on a new belt). A light cue on either side of the animal was triggered at 40 cm (flashing 10 Hz for 500 ms) that predicted the reward location at 100 cm when activated on the left side and 160 cm when activated on the right side. Trials for each location were grouped in epochs of 12-18 laps and randomly switched. Mice performed one session per day of this task for a succession of 7 days.

Two-photon Ca^{2+} longitudinal image acquisition and signal processing

All Ca^{2+} imaging recordings were performed in the dark using a custom-made two-photon microscope (Janelia MIMMS design). Transgenetically expressed GCaMP6f was excited at 920 nm (typically 40 – 60 mW) by a Ti:Sapphire laser (Chameleon Ultra II, Coherent) and imaged through a Nikon 16x, 0.8 Numerical Aperture (NA) objective. Emission light passed through a 565 DCXR dichroic filter (Chroma) and was detected by GaAsP photomultiplier tubes (11706P-40SEL, Hamamatsu). Images (512 × 512 pixels) were acquired at ~30 Hz using the ScanImage software (Vidrio Technologies, LLC).

A reference field of view (FOV) was chosen and registered before the start of the experiment for every animal. Each day, the FOV was aligned to this reference and the experiment aborted if differences were noted in the imaging plane on subsequent days. Acquired two-photon images were motion-corrected using Suite2p[34] (Python version, https://github.com/MouseLand/suite2p). Images were registered across days and only data from mice with stable FOVs across 7 days was considered for further processing. Image Segmentation into regions of interest (ROIs) to identify neuronal somata was done manually in ImageJ (version 2.3.0) to ensure that each ROI could be reliably tracked across all days. Briefly, frames were subsampled from across all sessions to form a composite image across days. Image segmentation was performed on this composite image with subsequent manual verification that every ROI adequately and exclusively represented the given cell on each day. Signal extraction was performed using custom code in Python (scipy.ndimage).

The raw fluorescence was converted to Δf/f, where Δf/f was calculated as (F – F0)/F0, where F0 is the 50th percentile of a 25-s moving window. Only significant Ca^{2+} transients, defined as transients larger than 3 Standard Deviations above the baseline noise were considered as functional activity for any further analysis. Baseline noise was estimated from deviations below peak histogram values of all Δf/f activity.

Determination of Place Field Activity

Spatial maps of neural activity were formed by dividing the 180 cm track into 50 spatial bins of 3.6 cm each. For each spatial bin, for every lap, the mean Δf/f was calculated when the velocity of the animal was above 2cm/s.

A behavioral epoch was determined to have place field (PF) activity if 1) Spatial Activity in the epoch had spatial information that exceeded 95% confidence interval determined by shuffling the epoch activity as previously described[23,35]. 2) Only laps with peak Δf/f within 30 cm of the peak average epoch activity were considered for further PF analysis. 3) An onset lap could be determined as the first instance where 3/5 laps showed PF activity. 4) The reliability of PF activity after the onset lap was 40% for the rest of the epoch.

The PF location for a given reward location was determined as the peak of the average lap activity for all laps within the active behavioral epochs for that reward location.

Determination of day-to-day Place Field stability criteria and stability index

To determine the amount of day-to-day PF shifting or jitter that should be tolerated for a PC to be considered as having a consistent PF we generated a distribution of the day-to-day COM shifts of the population of PCs. This distribution was generally normal (however, with a slight negative shift from zero) and thus was fit with a gaussian function from which 3 SD was found to be 25 cm (Extended Data Fig. 2a). Based on this we used a window of ±30 cm to fully capture the PCs within this central process. Thus, to be considered a stable PC the neuron had to express a consistently active PF on each consecutive day as defined by its COM being within 30 cm of that on the first day of appearance. We calculated the expected results (as in Fig. 2a) of a random, memory-less, process that used the ±30 cm window of COM jitter ($A \cdot 0.3^{d} \cdot 0.33^{d-1}$). Where A is the available population of neurons on a given day (starts at 2511 on day 1 and decreased as A minus pastPCs on a given day), 0.3 is the probability of any particular neuron becoming a PC (given the fraction of average PC count and total imaged neurons or 767/2511), 0.33 is the jitter

window (60 cm/180cm) and d is the day of the "recording". The difference between the analysis shown in Extended Data Fig. 3B and that in Fig. 2a gives confidence that using the ±30cm window does not cause our data to be heavily impacted by a random process. Finally, we analyzed the PC data using a ±20 cm window and found that although there were fewer PCs in the stable populations the data were still well fit by a double exponential with similar time constants as found using the ±30 cm window (Extended Data Fig. 3c). We surmise that the tighter window slightly reduced the time constants as more PCs were removed from the stable groups on later days because they had shifted outside the window for one day during the week (even if they returned the next day; see SFig. 3E, cell 909). In this way the tighter time window can be viewed as overly restrictive.

For calculations of sustained and transient PC numbers (Fig. 2) we identified transient cells as those that had a stable PF for 1 or 2 days (≤2 days) and sustained as those with a stable PF for 3 or more days (>2 days). For calculations of sustained and transient PC properties (Figs. 3 &4) we identified transient cells as those that had a stable PF for 1 day (1 day) and sustained for 3 or more days (>2 days). We based this on accuracy data from the model shown in Extended Data Fig. 3i&j. This later criterion gave less accurate PC counts but more accurate properties since there was a reduced misidentification.

PF stability index was the fractional difference between the number of PCs per mouse that had a minimum level of shift (<20 cm) and that expected from random. To calculate this we subtracted the upper 99% confidence interval of a random distribution from the total number of PCs with a two-day interval (d versus d+2) shift <20 cm (1st three 5 cm bins) then divided this by the total number of PCs in that mouse for the given day (Extended Data Fig. 5a).

Behavioral data quantification

The Velocity and Licking behavior was mapped into 50 spatial bins per running lap for quantification of behavior. For licking selectivity, the probability of licking at a given location bin was quantified as the percentage of laps with at least one lick inside the given spatial bin for the entire session. The reward anticipatory zone was defined as 3 bins before reward location and the random zone consisted of any 3 bins not overlapping the active or alternate reward zone. Licking Selectivity was quantified as

$$Licking\ Selectivity = \frac{P_{lick}(Anticipatory\ Reward\ Zone) - P_{lick}(Random\ Zone)}{P_{lick}(Anticipatory\ Reward\ Zone)}$$

Trial-by-trial Cosine Similarity and Discrimination Indices

Cosine Similarity Matrices for individual cells and across population were calculated as previously described[36]. Briefly, for the Cosine Similarity Matrix of an individual cell, every row of the cell's spatial activity map, $\tilde{A}$, was divided by its l_2 norm to give the matrix $\bar{\tilde{A}}$. The cosine similarity matrix for each cell is then given by $\tilde{C} = \bar{\tilde{A}}\bar{\tilde{A}}^T$. For Population Similarity matrices, the single cell spatial activity maps were horizontally concatenated to form a fat matrix $A = [\, A_1 | A_2 | \ldots | A_N]$, where N is the number of neurons recorded in that session. Each row of A was divided by its l_2 norm to give the matrix $\bar{A}$. The Population Similarity Matrix was then given by $C = \bar{A}\bar{A}^T$.

The Cellular Discrimination Index was calculated for each cell from $\tilde{C}$. For each row of $\tilde{C}$, the average 'within RL' cosine similarity per row was calculated as the average value from all trials of the same reward location and 'between Rl' cosine similarity per row, as the average value from all trials of the alternate reward location. The difference in the within RL and between RL averages across all rows was deduced as the Cellular Discrimination Index (CDI). The Population Discrimination Index (PDI) was likewise calculated using the Population Similarity Matrix, C as the starting matrix.

BTSP Analysis

A putative BTSP event was identified as 1) a strong Calcium event that had an amplitude in the top 20th percentile for all Calcium events in that cell for a given session. 2) Only laps with peak Δf/f within 30 cm of the putative BTSP event peak were considered for further BTSP analysis. 3) the event associated with 4/5 subsequent laps actively firing, and 4) an amplitude increase of 50% when the activity of following 5 laps was compared to that of the preceding 5 laps. The values for all BTSP related events with respect to peak, duration, location were determined in the time domain and not from the average spatial activity maps.

Pharmacology during two-photon imaging

For the local pharmacology experiments, the animal was briefly anesthetized >120 minutes before the recording session using isoflurane. The hippocampal window was carefully punctured (~100 µm-wide hole) near the imaging field of view and then covered with a silicone elastomer (Kwik-Cast). This procedure lasted about 5-10 min. The animal was allowed to recover at least 120 mins. Thereafter, the animal was positioned under the two-photon microscope, the Kwik-Cast plug was

removed, and the cannula was filled with D-APV (50-75 μM) dissolved in sterile saline or with sterile saline alone. The animal was prevented from running for initial 10 mins to allow for diffusion of the drug. APV or saline was present in the cannula throughout the remainder of the recording session.

Computational model

To simulate the production of two groups of active PCs with distinct PF activity decay rates we used a standard first order competitive interaction between three cellular pools, which modelled (1) available pyramidal cells, (2) transient cells and (3) sustained cells, as schematized (Extended Data Fig. 3). The reactions were separated into two phases to reproduce the two components of the behavior (time on- and off-track). Forward rate equations (activations) were:

$$\frac{d[A]}{dt} = -(\mathrm{k1} + \mathrm{k2})[\mathrm{A}];$$

$$\frac{d[T]}{dt} = \mathrm{k1}[A];$$

$$\frac{d[S]}{dt} = \mathrm{k2}[A];$$

where initial [A] was 2511 and dt was 0.01 hour for 100 time steps (1 hour). After which the elements were allowed to decay back to the available population for an additional 2300 time steps (23 hours) according to rate equations (decay)

$$\frac{d[T]}{dt} = -\mathrm{k3}[\mathrm{T}];$$

$$\frac{d[S]}{dt} = -\mathrm{k4}[\mathrm{S}];$$

$$\frac{d[A]}{dt} = \mathrm{k3}[\mathrm{T}] + \mathrm{k4}[\mathrm{S}];$$

Rate constants (k1, k2, k3, k4) are shown in Extended Data Fig. 4. The values of each of these were determined from the data where k3 and k4 were set by the fast and slow time-constants, respectively, produced in Fig. 2. [A] was initialized to the total number of imaged neurons. k1 and k2 by the initial, fractional amplitude of the slow component (Amp2) determined in Figure 1.

Initial [A] = 2511

$$k1 = ln\left(\frac{2511-\text{total PCs day1}}{2511}\right) \cdot \left(\frac{Amp1}{Amp1+ Amp2}\right);$$

$$k2 = ln\left(\frac{2511-\text{total PCs day1}}{2511}\right) \cdot \left(\frac{Amp2}{Amp1+Amp2}\right);$$

$$\mathrm{k3} = \frac{1}{\tau 1};$$

$k4 = \frac{1}{\tau 2}$;

To reproduce multiple days of on- and off-track experience, repeated activations and decays were given and k1 and k2 were scaled daily by the fraction of the population present at the beginning of each day and the desired daily total population from data

$k1 \times a; \quad a = 1 - \left(\frac{[S]_d + [T]_d}{expected\ daily\ total\ PCs}\right)$; where d is day.

$k2 \times b; \quad b = a \times 0.6.$

b was the only free parameter in the model and was adjusted to minimize MSE between the model results and the data shown in Fig. 2a.

To generate the data to compare with that in Fig. 2a we ran the model for single day activations, starting at day 1 and progressing through day 7. The daily values of k1, k2 and [A]t calculated from the multiple day run of the model were used. To determine how well the model corresponded to the data we calculated residuals (total residual= -10.1; n=28) and mean squared error (MSE= 182; n=28) between the model results and the 28 data points shown in Fig. 2a (Fig. 2g).

Statistical methods.

The exact sample size (n) for each experimental group is indicated in the figure legend or in the main text. No statistical methods were used to predetermine sample sizes, but our sample sizes are similar to those reported in previous publications[10,23,37] using a similar behavioral task and by the expected number of active neurons that can be imaged with the two-photon microscope in awake behaving mice. Normality for data was tested with a Kolmogorov-Smirnov test before using any parametric statistical testing. If not otherwise indicated in the figure, data are shown as mean ± SEM.

Supplementary references

34) Pachitariu, M. *et al.* Suite2p: beyond 10,000 neurons with standard two-photon microscopy. *BioRxiv* (2017).

35) Gauthier, J. L. & Tank, D. W. A Dedicated Population for Reward Coding in the Hippocampus. *Neuron* **99**, 179-193 e177, doi:10.1016/j.neuron.2018.06.008 (2018).

36) Plitt, M.H., Giocomo, L.M. Experience-dependent contextual codes in the hippocampus. *Nat Neurosci* **24**, 705–714 (2021). https://doi.org/10.1038/s41593-021-00816-6

37) Cholvin, T., Hainmueller, T. & Bartos, M. The hippocampus converts dynamic entorhinal inputs into stable spatial maps. *Neuron* **109**, 3135-3148 e3137, doi:10.1016/j.neuron.2021.09.019 (2021).

Acknowledgements
We thank S. Romani for helpful discussions and C. Grienberger, S. Romani and H. Zoghbi for comments on the manuscript. This work was supported by the Howard Hughes Medical Institute and the Cullen Foundation. The data that supports the findings of this study are available from the corresponding author upon request. The code that supports the findings of this study is available from the corresponding author upon request.

Author contributions
S.V., R.C. and JCM designed experiments. S.V. performed experiments. S.V. and JCM analyzed data. JCM created the model. S.V and JCM wrote the manuscript with comments from RC.